metals

MDPI

Article

Quantification of Hydrogen Flux from Atmospheric Corrosion of Steel Using the Scanning Kelvin Probe Technique

Flavien Vucko *, Varvara Shubina Helbert and Andrei Nazarov

French Corrosion Institute, RISE (Research Institutes of Sweden), 29200 Brest, France; varvara.helbert@institut-corrosion.fr (V.S.H.); andrei.nazarov@institut-corrosion.fr (A.N.)
* Correspondence: flavien.vucko@institut-corrosion.fr

Abstract: The atmospheric corrosion of high-strength steels can lead to hydrogen absorption directly linked to hydrogen embrittlement or delayed fracture phenomena. A scanning Kelvin probe (SKP) and electrochemical permeation technique (EPT) were applied to correlate the potential of an oxidized surface with the flux of hydrogen across a thin steel membrane. The side of the membrane opposite the corroding or electrochemically charged area was analyzed. The potential drop in the oxide was calibrated in terms of surface hydrogen activity, and SKP can be applied in situ for the mapping of hydrogen distribution in the corroding metal. A very low flux of hydrogen can be characterized and quantified by SKP, which is typically observed under atmospheric corrosion conditions. Therefore, hydrogen localization that drives steel durability under atmospheric corrosion conditions can be evaluated.

Keywords: scanning Kelvin probe; steel; hydrogen; corrosion

Citation: Vucko, F.; Helbert, V.S.; Nazarov, A. Quantification of Hydrogen Flux from Atmospheric Corrosion of Steel Using the Scanning Kelvin Probe Technique. *Metals* **2023**, *13*, 1427. https://doi.org/10.3390/met13081427

Academic Editor: Jianqiang Wang

Received: 19 June 2023
Revised: 4 August 2023
Accepted: 8 August 2023
Published: 9 August 2023

1. Introduction

During service life, components and the structure of vehicles can be submitted to severe corrosion conditions, particularly in areas where de-icing salts are used during winter periods [1–3]. Under such conditions, corrosion-induced hydrogen uptake can lead to severe damage to high-strength steels [4–7]. Indeed, the mechanism of hydrogen embrittlement is strongly linked to the quantity of hydrogen, in particular diffusible hydrogen, that interacts with the microstructure and mechanical field [8–10]. Test methods combining lateral resolution, time-resolved data, and quantification are required to determine the critical hydrogen content or hydrogen activity that leads to hydrogen embrittlement.

Based on the electrochemical permeation technique (EPT), Omura et al. [11] showed that hydrogen can enter steel during the wetting or drying steps of a corrosion cycle. The amount of permeated hydrogen showed a strong dependence on temperature, relative humidity, and surface salt contamination (quantity and composition). Similar results have been reported by Ajito et al. [12], who monitored permeation current and potential in a drying droplet of salt water. The flux of hydrogen is at its maximum at the end of the drying process and relates to the increase of local acidity in the anodic sites on the steel surface. With additional corrosion cycles, the formation of the corrosion products tends to mitigate pH reduction, decreasing the activity of hydrogen [12]. Increasing the concentration of salt in the droplet enhances the anodic dissolution and consequently increases the flux of hydrogen [12]. For mobile conditions, using a specific EPT system, Ootsuka et al. [13] showed that the amount of absorbed hydrogen in steel on wet roads is related to the corrosion rate of steel. However, the amount of hydrogen absorbed by steel results from a complex combination of the driving state of the vehicle (parking or moving), chloride loading, eventual washing of surfaces, and road-surface conditions.

In the case of the generalized corrosion mechanism, a hydrogen concentration of 0.2 ppm was found in high-strength steel using the hydrogen thermo-desorption spectroscopy (TDS) technique [14]. For another high-strength steel, QP1180, a concentration of

around 0.3 ppm of diffusible hydrogen was measured [15]. An even lower range of hydrogen activity can be found in the literature under atmospheric corrosion conditions [16,17]. Hydrogen activity as low as 0.003 ppm has been obtained by an EPT method during the monitoring of wet–dry transients [17].

Most previous data have been obtained using quantitative methods with overall concentration detected, such as EPT and TDS methods. Some recent studies have suggested that the scanning Kelvin probe (SKP), or scanning Kelvin probe force microscopy (SKPFM), is the most sensitive technique to detect extremely low quantities of hydrogen [18,19]. Using the SKP method, Rudomilova et al. [20] showed that generalized corrosion led to lower hydrogen activity compared to localized corrosion, which can greatly promote hydrogen absorption into steel during atmospheric corrosion processes. Therefore, a technique with sufficient lateral resolution is necessary to accurately assess the critical hydrogen activity that would lead to the service failure of high-strength steels [21,22]. Indeed, hydrogen generated under atmospheric corrosion conditions can lead to the failure of advanced high-strength steels [23–25]. The presence of a coating, in particular zinc-based coatings, can further affect the resistance of steel to environmentally assisted failure [26].

The SKP method is now a well-established technique to qualitatively visualize the hydrogen distribution in various metals [27–33]. For bare steel, hydrogen permeating the membrane interacts with the native oxide film on the detecting side [34], which directly impacts the measured Volta potential, leading to a potential drop. The potential is also affected by the re-oxidation of the oxide film due to the interaction with the oxygen in the air [32,34]. Consequently, a direct evaluation of hydrogen activity is not possible without the calibration of the potential variation using a quantitative method. In this case, EPT is probably the most adapted method due to its very high sensitivity to measuring hydrogen flux [35].

Using the SKP, potential maps related to the distribution of hydrogen can be obtained [6,27,30,32]. These potential maps can be converted into maps of hydrogen concentration or hydrogen activity with a time-resolved process. In such cases, the distribution of diffusible hydrogen and hydrogen trapped locally in cracks or inclusions can be observed. As shown recently [32], the attraction of hydrogen to locations with elevated tensile stress has also been observed by SKP. However, these results were only qualitative observations, and it is preferable to transform this potential into quantitative values in terms of hydrogen concentration.

The objective of the study was to demonstrate the possibility of using the SKP method to quantify very low hydrogen flux with a spatial resolution compatible with atmospheric corrosion mechanisms. To do so, a specific setup was developed for the in situ hydrogen charging of a steel membrane directly in the SKP chamber. The membrane was coupled with a galvanostat for direct calibration of the signal by EPT tests, which were performed under the same charging conditions. Similar experiments were also performed using ex situ charging, followed by immediate SKP mapping. Finally, the hydrogen flux from corroding steel under a droplet of NaCl was monitored and quantified by SKP.

2. Materials and Methods

2.1. Materials and Specimens

A ferritic carbon steel DC04 was used for analyses. Its chemical composition is indicated in Table 1.

Table 1. Chemical composition of the DC04 steel (wt.%).

Fe	C	Mn	P	S
Bal.	<0.08	<0.4	<0.03	<0.01

Flat samples were cut from 0.8 mm plates, and their thickness was further reduced to roughly 0.5 mm by grinding and polishing using a final step with P4000 SiC paper. Then,

for SKP measurements, thermal treatment at 100 °C was applied for 1 h to stabilize and calibrate the oxide film, which greatly facilitates SKP investigations. After heat treatment, the oxide at the entry side (exposed to cathodic charging or corrosion) was removed by polishing with P4000 SiC paper. For EPT experiments, a palladium layer was deposited on the detecting side by an electro-deposition process in $PdCl_2$ ammoniacal solution [36]. The plating conditions were adjusted to obtain a palladium layer thickness of around 200 nm.

2.2. EPT Measurements

EPT experiments were conducted using standard Devanathan–Stachurski cells [37]. Briefly, the steel membrane was fixed between two electrochemical cells using O-rings from both sides. From the entry side, hydrogen charging was performed in 5 wt.% NaCl solution at 20 °C using cathodic current densities, from 50 µA/cm^2 up to 5 mA/cm^2. The hydrogen detection side was made on the Pd-coated side, i.e., from the opposite side of the membrane in 0.1 M NaOH solution. The area of the Pd-plated side in contact with the NaOH solution was 0.93 cm^2. The counter-electrode was a TiMMO (mixed metal oxide) wire with a large surface area, and the reference electrodes were a saturated calomel electrode (Hg/Hg_2Cl_2, E = 0.241 V vs. SHE—standard hydrogen electrode) and a mercury oxide Hg/HgO electrode in 0.1 M NaOH (E = 0.165 V vs. SHE). The Pd-plated surface of the steel specimen was polarized at +200 mV vs. Hg/HgO using a potentiostat until the background current was stabilized. Then, the entry side was filled with NaCl solution, and hydrogen cathodic charging was started immediately.

A multichannel potentiostat/galvanostat Origaflex OGR-500 (Origalys, Lyon, France) was used for both potential monitoring during cathodic current application on the entry side and for hydrogen permeation current recordings from the opposite side of the membrane. From the permeation results, the subsurface hydrogen concentration was calculated using the stabilized permeation currents [38].

2.3. SKP Procedure

SKP experiments were conducted with height-controlled instruments from Wicinski and Wicinski (Erkrath, Germany). A Ni–Cr alloy needle with a tip diameter of 130 µm was used as the reference electrode. The distance between the probe and the specimen was kept constant (50 µm) during the SKP mappings, thanks to simultaneous topography and potential measurements. A vibration amplitude of 20 µm at a frequency of 1 kHz was set. The measurements were performed at a temperature of 22 ± 1 °C and ambient humidity of 50–60% RH.

The potential of the SKP probe was systematically calibrated using a saturated $Cu/CuSO_4$ electrode before each experiment and verified at the end of the measurement by the same method. The hardware of the SKP equipment was upgraded to reduce the noise linked to the use of a galvanostat for the in situ cathodic charging. Hydrogen charging was carried out using the setup described in Figure 1.

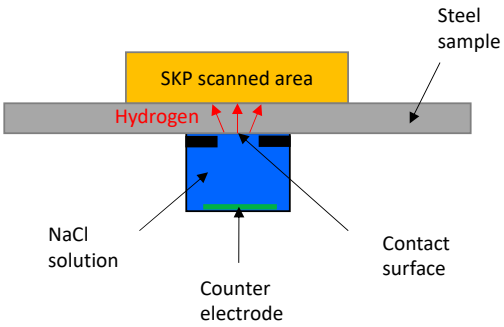

Figure 1. Setup for SKP measurements under hydrogen-charging conditions.

Ex situ experiments were also conducted using a similar setup to EPT. To limit hydrogen bubbling during cathodic charging, as the charging side was facing down during in

situ charging, the maximum charging current was limited to 150 µA/cm^2. This was not an issue for ex situ charging, as hydrogen bubbles could easily escape from the charging surface when facing up. Most of the experiments were conducted in the range of 0–200 µA/cm^2, leading to rather low hydrogen uptake under atmospheric corrosion conditions.

To check the ability of the SKP technique to quantify hydrogen flux from atmospheric corrosion, a second SKP setup was designed using an NaCl droplet instead of the small reservoir with NaCl solution from Figure 1. The volume and concentration of the NaCl droplet were controlled to obtain surface contamination of 3 g/m^2. Sequential mappings of the detecting side were performed, and the potential drop was evaluated. The hydrogen activity from the corrosion induced by the droplet was determined.

3. Results and Discussion

3.1. Hydrogen Activity under Cathodic Charging Conditions

EPT experiments were conducted under cathodic charging conditions to quantify the concentration of the diffusible hydrogen at the entry side of the permeation membrane, which characterizes the efficiency of the hydrogen entry into the metal [38], also called subsurface hydrogen concentration C_0 or hydrogen activity. An average hydrogen diffusion coefficient was directly extracted from the permeation transients [35], as illustrated in Figure 2a. Then, the subsurface hydrogen concentration was calculated using Equation (1):

$$C_0 = \frac{i_p^{\infty} \times L}{F \times D} \quad (1)$$

where D is the hydrogen diffusion coefficient (5.0×10^{-10} m^2/s), L is the thickness of the membrane, F is the Faraday constant, and $i_p{}^{\infty}$ is the steady-state permeation current. The density of the steel is required to convert the data into ppm.

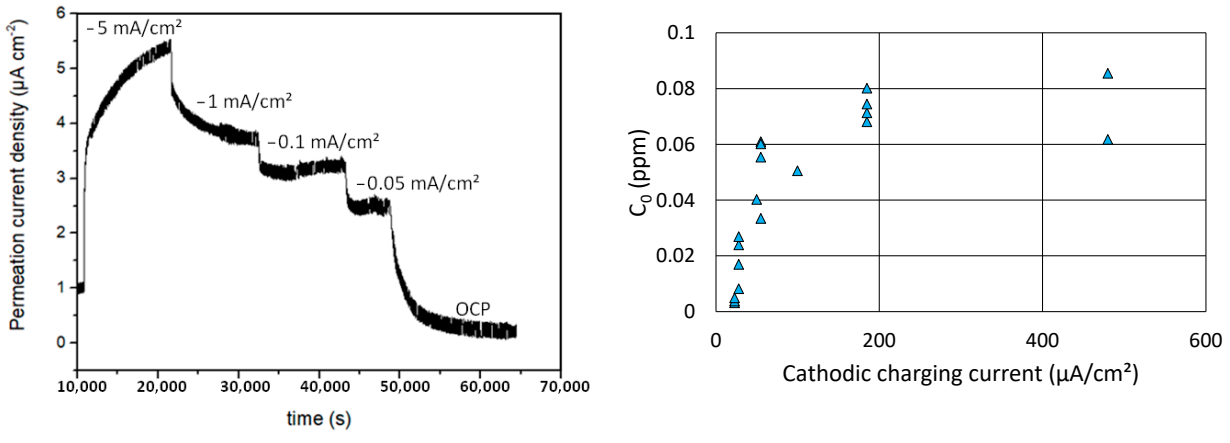

(**a**) (**b**)

Figure 2. (**a**) Permeation transients under different cathodic charging current densities, and (**b**) the relationship between hydrogen subsurface C_0 concentration and cathodic current density, determined from EPT experiments.

As illustrated in Figure 2a, the transient method was used to obtain several subsurface hydrogen values from a single sample. Three steel membranes with very similar thicknesses (0.5 ± 0.02 mm) were studied to plot the data presented in Figure 2b.

As shown, C_0 rapidly decreased with increasing charging current density. In theory, hydrogen production would be directly proportional to charging current [39]. However, surface conditions can greatly affect hydrogen uptake and therefore permeation current. Indeed, as shown in [40], the ratio between permeation and charging currents systematically decreased when charging current increased. This can be related to the coverage of the steel surface by the adsorbed hydrogen as a function of the rate of water reduction. Then,

electrochemical (Heyrovsky reaction) and/or chemical (Tafel reaction) hydrogen desorption reactions can become dominant, limiting the increase of hydrogen uptake.

Investigations were conducted in situ using the SKP to map the potential distribution at the opposite side, similar to the EPT tests. The charging current was kept constant throughout the whole test for in situ charging conditions. Therefore, one sample was used for each cathodic charging level. An example of a stabilized potential map for a charging current of -100 µA/cm^2 is presented in Figure 3a. The initial potential of the steel before cathodic charging, related to the passive state, was in the range of 300–350 mV/SHE. After 1 h of hydrogen charging from the opposite side, a potential drop was observed directly opposite the charging area. Then, the stabilized potential drop was obtained within 2 to 3 h. The size of the area affected by hydrogen permeation at the detection side corresponded to the size of the charging area in contact with the solution. For longer charging time, only a slight increase in the size of the affected zone was observed, which was probably related to the lateral hydrogen diffusion.

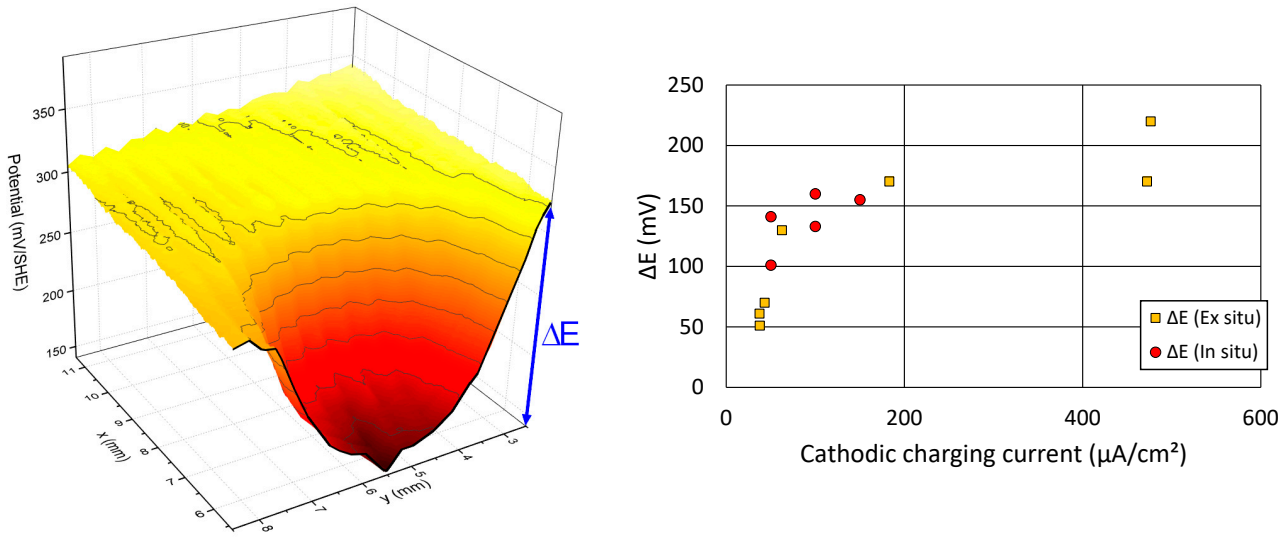

(**a**) (**b**)

Figure 3. (**a**) SKP potential map under hydrogen-charging conditions at -100 µA/cm^2, and (**b**) evolution of the potential drop measured by SKP as a function of cathodic charging current.

The stabilized potential drop was calculated for each map from the potential of the passive state of the steel surface that was not affected by permeated hydrogen and the potential affected by hydrogen permeation, as described in [6,33] and shown in Figure 3a. Some of the experiments were also carried out ex situ to compare with in situ measurements. Under these conditions, charging in the electrolyte was carried out for 2 h and SKP analysis of the detecting side was obtained within 15 min of the end of the cathodic charging. To do so, the maps were carried out from the center of the samples, corresponding to the center of the charging area, and only a quarter of the sample was mapped. Moreover, the scan steps were set at 100 and 500 µm for the x and y directions, respectively. The resolution of the potential maps under these conditions was enough to calculate the potential drop.

All the obtained results are plotted in Figure 3b. The potential drop induced by hydrogen followed a power-law evolution as a function of the cathodic charging current, similar to the hydrogen activity obtained by EPT in Figure 2b.

Very similar results were obtained when using ex situ or in situ cathodic charging (Figure 3b). Such behavior was linked to the mechanism of hydrogen detection by SKP [33]. Indeed, SKP is sensitive to the oxidation state of oxide film, which is driven by a competition between the reduction reaction from the permeated hydrogen and oxidation from ambient oxygen [34]. The re-oxidation kinetic was found to be rather slow [32]; therefore, the potential drop remained stable over a rather long time in laboratory air conditions. For

an even higher cathodic charging current in the range of 1 to 10 mA/cm^2, the potential drop seemed to be limited to around 250 mV, as also observed in [32]. Detection conditions, under laboratory air and not in an inert gas such as nitrogen, might slightly limit the ability of SKP to quantify higher hydrogen fluxes.

An additional experiment was conducted with SKP potential monitoring at a single location in the center of the area affected by hydrogen permeation. Charging transient and permeation current monitoring was applied in the EPT experiments. Under such conditions, the kinetic of the potential drop evolution detected by SKP was slower than for EPT, as shown in Figure 4. This kinetic was even slower during a decay transient after a reduction of the charging current density, as illustrated in Figure 4b.

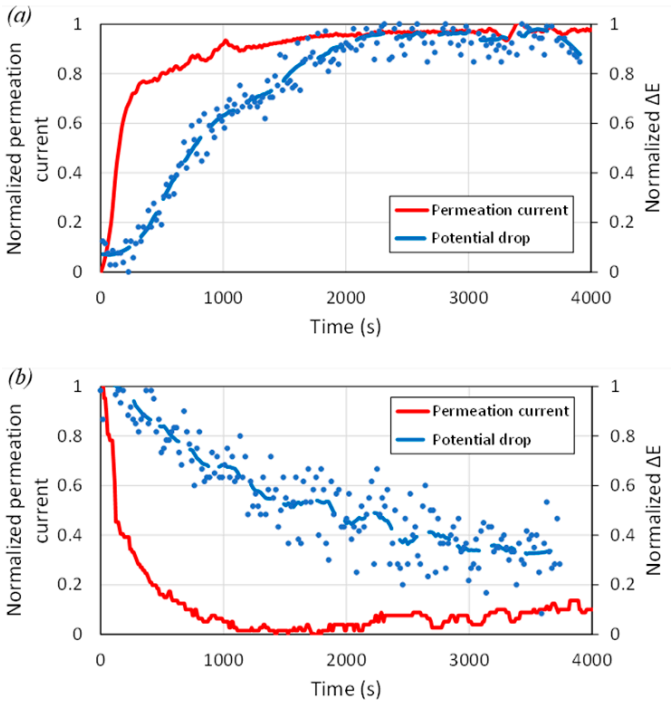

Figure 4. (**a**) Rise and (**b**) decay transients obtained with EPT (permeation current) and SKP (ΔE). The values were normalized by the maximum and minimum values obtained during the transients.

SKP and EPT experiments were carried out at electrochemical potentials in the range of 0–200 mV/SHE related to the similar thermodynamics of electrochemical reactions. The range of potential corresponds to steel passivity, and that passive state was affected by hydrogen. For these two methods, the principles of sensing and surface conditions are quite different. SKP measurements were done under air conditions, with easy access to oxygen for the surface of the steel. Therefore, reactions of oxygen with the oxide film and eventually directly with effused atomic hydrogen can be expected. Consequently, the transient (Figure 4a) and surface oxide conditions are affected by reduction reactions of both permeated hydrogen and oxide re-oxidation by the oxygen in the air, which finally delays the stabilization of the potential. In particular, the difference was enhanced in the case of the decrease in hydrogen activity, which would support a slow kinetic of the re-oxidation reactions of the oxide layer under such conditions. Further investigations should be conducted to fully characterize this phenomenon and improve the correlation of the transients by creating experimentally more similar SKP and EPT detection conditions. In this study, as the correlations were only based on the stabilized values, these kinetic transient effects were expected to have no impact.

3.2. Calibration of SKP Potential Drop by EPT

EPT and SKP experiments were conducted using low hydrogen-charging conditions, in NaCl solution at neutral pH, without promoters of hydrogen uptake. In particular,

the charging current was set low, mainly in the range of 50–200 μA/cm^2. Under such conditions, the saturation of the steel with hydrogen cannot be reached, so hydrogen entry conditions were not limited by bulk hydrogen concentration. Therefore, the detection of hydrogen flux by both EPT and SKP tests was influenced only by the concentration of hydrogen on the entry side. Moreover, no surface damage, such as blisters, was observed under all investigated conditions, which would have revealed some over-saturation effects for such low-grade steel.

During SKP experiments, several mechanisms can occur on the detecting side. As shown by XPS investigations, iron oxide film was partially reduced by permeated hydrogen [33]. Then, the recombination of atomic hydrogen into gas molecules on the detecting side of the specimens can also occur, even if the probability would be low for small hydrogen flux and in the presence of an oxide at the surface of the sample. A contribution from the direct interaction of hydrogen with the oxygen in the air at the oxide–steel interface could be considered, as bigger potential changes were observed in the nitrogen atmosphere [6]. Finally, it could be assumed that the thin iron oxide layer of a few nanometers was not a barrier in the overall process of hydrogen desorption. Consequently, it was expected that the subsurface hydrogen concentration at the detecting side of SKP samples was close to zero. Therefore, the boundary conditions of both EPT and SKP experiments, in terms of hydrogen diffusion, should be similar. However, SKP measurements (e.g., Figure 4a) in an inert atmosphere might increase the relationship between the two methods.

The potential drop obtained by SKP and the hydrogen activity calculated from EPT experiments are directly superimposed in Figure 5. As a first approach, a linear relationship can be built between the two parameters, at least in the range of low-charging-current densities. A deviation from this linear relationship could be observed for higher charging current densities (or hydrogen activities).

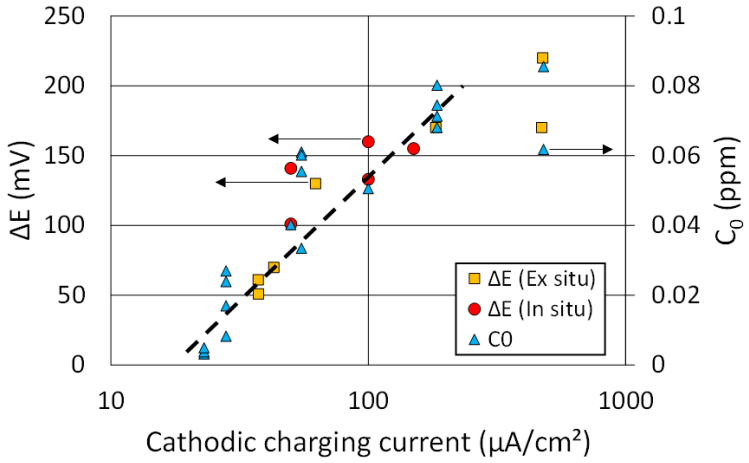

Figure 5. Evolution of the potential drop (ΔE) and the hydrogen activity (C_0) as a function of the cathodic charging conditions.

From the results presented in Figure 5, it can be seen that the detection limit of the SKP method would be rather good, with sensitivity to hydrogen activity as low as 0.01 ppm of hydrogen. Therefore, the SKP technique is a very sensitive tool to quantify the very low hydrogen uptake that is typically encountered in atmospheric corrosion studies. However, to fully exploit such data, a model of hydrogen distribution should be used to calculate the hydrogen content in critical areas, such as mechanically stressed areas, knowing the boundary conditions of hydrogen uptake thanks to SKP tests.

3.3. Hydrogen from Corroding Droplet

SKP mapping was performed in situ during the atmospheric corrosion of the steel surface under 0.1 M NaCl droplet. Based on the size of the deposited droplet, a surface contamination of 3 g/m^2 was obtained. After an incubation time of roughly 15 h, a poten-

tial drop could be observed, as illustrated in Figure 6a. Interestingly, the potential drop was located precisely at the location of the droplet on the opposite side. The maximum potential drop on the detecting side corresponded to the center of the droplet on the corroding side, and not the periphery of the droplet or even further into the cathodic area. Under atmospheric corrosion conditions, a strong separation of anodic and cathodic sites is usually observed, particularly with NaCl solution [41,42]. Oxygen reduction is the main reaction at the cathode, controlling the overall corrosion process. As shown, no hydrogen is produced in this area, as the potential remained high on the detecting side out of the droplet location, corresponding to the passive state of the steel. On the contrary, at the anodic location, the development of red rust, associated with a decrease in pH hydrogen uptake, occurs. It could be assumed that very locally in the droplet, both anodic reactions of iron dissolution and the cathodic reaction of water reduction (facilitated by the local pH) occurred, these being the main sources of hydrogen for a bare steel surface under atmospheric corrosion conditions.

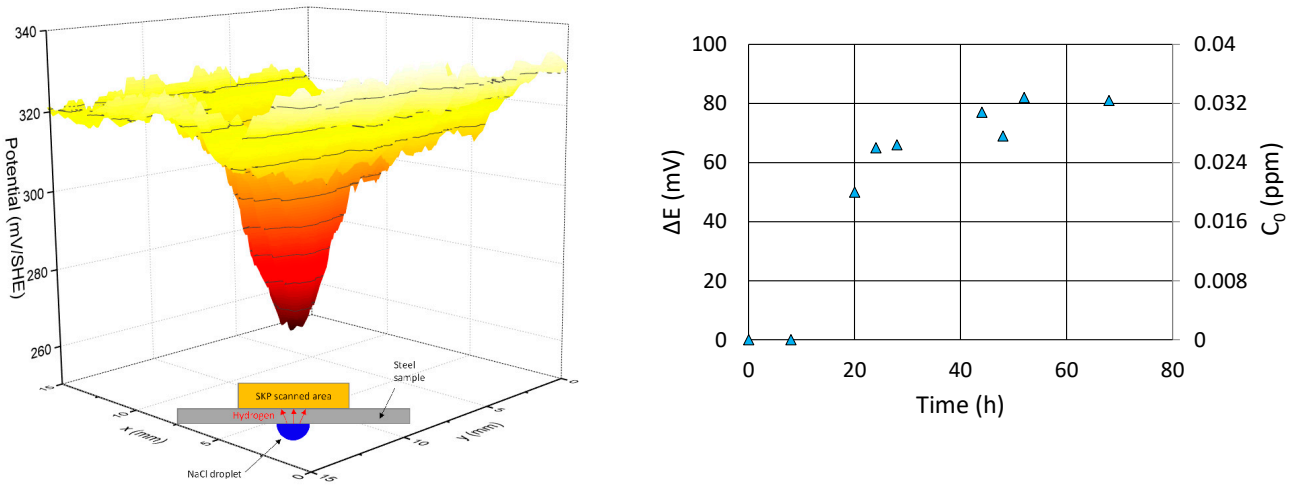

(**a**) (**b**)

Figure 6. (**a**) SKP map on the detecting side and (**b**) evolution of potential drop (ΔE) and hydrogen activity (C_0) during atmospheric corrosion with the NaCl droplet.

From the successive maps, the average potential drop was evaluated and the hydrogen activity from the corroding steel in the droplet was calculated using a linear relationship (Figure 5). As shown in Figure 6b, the hydrogen activity quickly increased after the incubation time, and reached a maximum value of 0.033 ppm after roughly 2 days of exposure. Such an amount was compatible with the literature data on different steels [17]. Therefore, the method was able to localize and quantify very low hydrogen activity related to mild atmospheric corrosion conditions. The potential decay in place of hydrogen effusion due to corrosion under the NaCl droplet was also observed in [6], where high-strength steel was investigated.

The anodic locations on the corroding steel surface are the sources of hydrogen that permeated the detecting side. The effect of galvanic zinc coating, which cathodically polarized the steel surface, on hydrogen distribution was also demonstrated [6,32]. Therefore, the correlation (Figure 5) can be helpful to approximate the hydrogen concentrations in results provided by previous studies. However, for the precise determination of hydrogen concentration and distribution, calibration using EPT is required, and the thickness of the specimens probably has a large impact on the correlation.

4. Conclusions

A hydrogen quantification protocol based on SKP and EPT has been developed to evaluate the hydrogen activity in corroding steel with some lateral resolution compatible

with atmospheric corrosion processes. From the results, the following conclusions can be drawn:

- A simple and fast calibration procedure was developed to quantify hydrogen activity using SKP detection on a thin steel membrane. The method is based on EPT transients and the measurement of SKP potential drop under similar cathodic charging conditions.
- Both ex situ and in situ hydrogen-charging procedures can be used to calibrate the SKP method. The potential of steel is mainly influenced by hydrogen flux. However, it is recommended that ex situ measurement be performed quite soon after the cathodic charging, using a fast scan rate (large steps). For in situ, a similar approach to EPT tests could also be developed, using charging transients, but with extended stabilization time.
- A linear relationship was found between the potential drop and hydrogen activity in the range of low charging currents and therefore low hydrogen activities. Some deviation from this linear relationship could be observed at higher charging current densities, because of the non-proportional increase of the hydrogen flux with increasing current for both EPT and SKP, due to the two different mechanisms.
- The obtained relationship between potential drop and hydrogen activity was valid only for the investigated steel with the defined thickness, structure, and hydrogen traps. To investigate new steel, the calibration procedure must be repeated.
- The calibrated SKP method shows a sensitivity even higher than 0.01 ppm for the quantification of the hydrogen activity. However, some saturation effect seemed to occur for higher charging current densities, at least under the applied test conditions.
- Due to competition between reduction and oxidation processes on the detecting side of the steel membrane analyzed by SKP, the diffusion coefficient of hydrogen should not be calculated from the evolution of the potential drop, even using in situ experiments. The exact mechanism responsible for this deviation has not been clarified.
- SKP can localize and quantify the hydrogen from a corroding steel membrane under mild atmospheric corrosion conditions. For bare steel, hydrogen is mainly produced at the anodic location of the atmospheric corrosion process due to local acidification.

As a perspective, the developed method can be used to assess the critical hydrogen uptake under atmospheric corrosion conditions that can lead to the hydrogen-assisted cracking of very high-strength steels. To do so, the hydrogen activity must be evaluated under representative atmospheric corrosion conditions, including potentially wet–dry transients. Further investigation is required to ensure the stability of the potential measurements under such conditions.

Author Contributions: Conceptualization, F.V. and A.N.; methodology, F.V. and V.S.H.; validation, F.V. and A.N.; formal analysis, F.V., V.S.H. and A.N.; investigation, V.S.H.; data curation, F.V.; writing—original draft preparation, F.V.; writing—review and editing, F.V., V.S.H. and A.N.; visualization, F.V. and V.S.H.; supervision, F.V. and A.N.; project administration, F.V.; funding acquisition, F.V. All authors have read and agreed to the published version of the manuscript.

Funding: This project has received funding from the Research Fund for Coal and Steel under grant agreement No 101034041.

Data Availability Statement: The data presented in this study are available on request from the corresponding author.

Conflicts of Interest: The authors declare no conflict of interest.

References

1. Mizuno, D.; Suzuki, S.; Fujita, S.; Hara, N. Corrosion monitoring and materials selection for automotive environments by using Atmospheric Corrosion Monitor (ACM) sensor. *Corros. Sci.* **2014**, *83*, 217–225. [CrossRef]
2. LeBozec, N.; Blandin, N.; Thierry, D. Accelerated corrosion tests in the automotive industry: A comparison of the performance towards cosmetic corrosion. *Mater. Corros.* **2008**, *59*, 889–894. [CrossRef]

3. Bednar, L. Automotive Body Component Field Corrosion Behavior in the De-Icing Salt Zone. In *SAE Technical Paper*; SAE International: Detroit, MI, USA, 1997; p. 971002.
4. Ćwiek, J. Hydrogen degradation of high-strength steels. *J. Achiev. Mater. Manuf. Eng.* **2009**, *37*, 193–212.
5. Nazarov, A.; Vucko, F.; Thierry, D. Scanning Kelvin Probe for detection of the hydrogen induced by atmospheric corrosion of ultra-high strength steel. *Electrochim. Acta* **2016**, *216*, 130–139. [CrossRef]
6. Schimo-Aichhorn, G.; Traxler, I.; Muhr, A.; Commenda, C.; Rudomilova, D.; Schneeweiss, O.; Luckeneder, G.; Duchaczek, H.; Stellnberger, K.-H.; Faderl, J.; et al. Hydrogen Insertion into Complex-Phase High-Strength Steel during Atmospheric Corrosion at Low Relative Humidity. *Metals* **2022**, *12*, 624. [CrossRef]
7. Nazarov, A.; Helbert, V.; Vucko, F. Scanning Kelvin Probe for Detection in Steel of Locations Enriched by Hydrogen and Prone to Cracking. *Corros. Mater. Degrad.* **2023**, *4*, 158–173. [CrossRef]
8. Robertson, I.M.; Sofronis, P.; Nagao, A.; Martin, M.L.; Wang, S.; Gross, D.W.; Nygren, K.E. Hydrogen Embrittlement Understood. *Metall. Mater. Trans. A* **2015**, *46*, 2323–2341. [CrossRef]
9. Popov, B.N.; Lee, J.-W.; Djukic, M.B. Hydrogen Permeation and Hydrogen-Induced Cracking. In *Handbook of Environmental Degradation of Materials*; Elsevier: Amsterdam, The Netherlands, 2018; pp. 133–162. [CrossRef]
10. Lyu, A.; Lee, J.; Nam, J.-H.; Kim, M.; Lee, Y.-K. Hydrogen absorption and embrittlement of martensitic medium-Mn steels. *Corr. Sci.* **2023**, *221*, 111304. [CrossRef]
11. Omura, T. Hydrogen Entry and its Effect on Delayed Fracture Susceptibility of High Strength Steel Bolts under Atmospheric Corrosion. *ISIJ Int.* **2012**, *52*, 267–273. [CrossRef]
12. Ajito, S.; Tada, E.; Ooi, A.; Nishikata, A. Simultaneous Measurements of Corrosion Potential and Hydrogen Permeation Current in Atmospheric Corrosion of Steel. *ISIJ Int.* **2019**, *59*, 1659–1666. [CrossRef]
13. Ootsuka, S.; Fujita, S.; Tada, E.; Nishikata, A.; Tsuru, T. Evaluation of hydrogen absorption into steel in automobile moving environments. *Corros. Sci.* **2015**, *98*, 430–437. [CrossRef]
14. Akiyama, E.; Matsukado, K.; Wang, M.; Tsuzaki, K. Evaluation of hydrogen entry into high strength steel under atmospheric corrosion. *Corros. Sci.* **2010**, *52*, 2758–2765. [CrossRef]
15. Zhao, Z.; Liu, M.; Zhou, Q.; Li, M. Hydrogen permeation behavior of QP1180 high strength steel in simulated coastal atmosphere. *J. Mater. Res. Technol.* **2022**, *18*, 2320–2330. [CrossRef]
16. Han, X.; Sakairi, M. The promotion effect of aluminium ion on hydrogen entry into steel during atmospheric corrosion. *Electrochim. Acta* **2023**, *458*, 142505. [CrossRef]
17. Ootsuka, S.; Tada, E.; Ooi, A.; Nishikata, A. Effect of Environmental Factors on Hydrogen Absorption into Steel Sheet under a Wet-dry Cyclic Corrosion Condition. *ISIJ Int.* **2021**, *61*, 1229–1235. [CrossRef]
18. Ma, Z.; Xiong, X.; Chen, L.; Su, Y. Quantitative calibration of the relationship between Volta potential measured by scanning Kelvin probe force microscope (SKPFM) and hydrogen concentration. *Electrochim. Acta* **2021**, *366*, 137422. [CrossRef]
19. Gruenewald, P.; Hautz, N.; Motz, C. Implementation of an experimental setup to qualitatively detect hydrogen permeation along grain boundaries in nickel using Scanning Kelvin Probe Force Microscopy under varying atmospheres. *Int. J. Hydrogen Energy* **2022**, *47*, 15922–15932. [CrossRef]
20. Rudomilova, D.; Prošek, T.; Ström, M. Hydrogen Entry into Steel Under Corrosion Products. *Corrosion* **2021**, *77*, 427–432. [CrossRef] [PubMed]
21. Wang, M.; Akiyama, E.; Tsuzaki, K. Determination of the critical hydrogen concentration for delayed fracture of high strength steel by constant load test and numerical calculation. *Corros. Sci.* **2006**, *48*, 2189–2202. [CrossRef]
22. Bergmann, C.; Mraczek, K.; Kröger, B.; Sturel, T.; Jürgensen, J.; Yagodzinskyy, Y.; Guo, X.; Vucko, F.; Kuhlmann, M.; Veith, S.; et al. *Hydrogen Embrittlement Resistance Evaluation of Advanced High Strength Steels in Automotive Applications*; SteelyHydrogen: Ghent, Belgium, 2018.
23. Akiyama, E.; Wang, M.; Li, S.; Zhang, Z.; Kimura, Y.; Uno, N.; Tsuzaki, K. Studies of evaluation of hydrogen embrittlement property of high-strength steels with consideration of the effect of atmospheric corrosion. *Met. Mater. Trans. A* **2012**, *44*, 1290–1300. [CrossRef]
24. Kim, H.-J.; Lee, M.-G.; Yoon, S.-C.; Vucko, F.; Lee, C.-W.; Theirry, D.; Kim, S.-J. Diffusible hydrogen behavior and delayed fracture of cold rolled martensitic steel in consideration of automotive manufacturing process and vehicle service environment. *J. Mater. Res. Technol.* **2020**, *9*, 13483–13501. [CrossRef]
25. Rudomilova, D.; Prošek, T.; Traxler, I.; Faderl, J.; Luckeneder, G.; Schimo-Aichhorn, G.; Muhr, A. Critical Assessment of the Effect of Atmospheric Corrosion Induced Hydrogen on Mechanical Properties of Advanced High Strength Steel. *Metals* **2020**, *11*, 44. [CrossRef]
26. Koul, M.G.; Sheetz, A.; Ault, P.; Repp, J.; Whitfield, A. Effect of Zn-Rich Coatings on the Corrosion and Cracking Resistance of High-Strength Armor Steel. *Corrosion* **2014**, *70*, 337–350. [CrossRef]
27. Nazarov, A.; Thierry, D. Corrosion and hydrogen entry into high strength steel. In situ SKP imaging of the hydrogen flux. In Proceedings of the 65th Annual Meeting of the International Society of Electrochemistry, Lausanne, Switzerland, 31 August–5 September 2014.
28. Schimo, G.; Burgstaller, W.; Hassel, A.W. Influence of atmospheric oxygen on hydrogen detection on Pd using Kelvin probe technique. *J. Solid State Electrochem.* **2018**, *22*, 495–504. [CrossRef]

29. Burgstaller, W.; Schimo, G.; Hassel, A.W. Challenges in hydrogen quantification using Kelvin probe technique at different levels of relative humidity. *J. Solid State Electrochem.* **2017**, *21*, 1785–1796. [CrossRef]
30. Schaller, R.F.; Scully, J.R. Measurement of effective hydrogen diffusivity using the Scanning Kelvin Probe. *Electrochem. Commun.* **2014**, *40*, 42–44. [CrossRef]
31. Evers, S.; Rohwerder, M. The hydrogen electrode in the dry: A Kelvin probe approach to measuring hydrogen in metals. *Electrochem. Commun.* **2012**, *24*, 85–88. [CrossRef]
32. Nazarov, A.; Vucko, F.; Thierry, D. Scanning Kelvin Probe Investigation of High-Strength Steel Surface after Impact of Hydrogen and Tensile Strain. *Corros. Mater. Degrad.* **2020**, *1*, 187–197. [CrossRef]
33. Vucko, F.; Ootsuka, S.; Rioual, S.; Diler, E.; Nazarov, A.; Thierry, D. Hydrogen detection in high strength dual phase steel using scanning Kelvin probe technique and XPS analyses. *Corros. Sci.* **2022**, *197*, 110072. [CrossRef]
34. Williams, G.; McMurray, H.N.; Newman, R.C. Surface oxide reduction by hydrogen permeation through iron foil detected using a scanning Kelvin probe. *Electrochem. Commun.* **2013**, *27*, 144–147. [CrossRef]
35. Zakroczymski, T. Electrochemical determination of hydrogen in metals. *J. Electroanal. Chem.* **1999**, *475*, 82–88. [CrossRef]
36. Manolatos, P.; Jerome, M. A thin palladium coating on iron for hydrogen permeation studies. *Electrochim. Acta* **1996**, *41*, 359–365. [CrossRef]
37. Devanathan, M.A.V.; Stachurski, Z. The Adsorption and Diffusion of Electrolytic Hydrogen in Palladium. *Proc. R. Soc. A Math. Phys. Eng. Sci.* **1962**, *270*, 90–102.
38. Zakroczymski, T. Adaptation of the electrochemical permeation technique for studying entry, transport and trapping of hydrogen in metals. *Electrochim. Acta* **2006**, *51*, 2261–2266. [CrossRef]
39. Akiyama, E.; Li, S. Electrochemical Hydrogen Permeation Tests under Conventional Potentiostatic Hydrogen Charging Conditions Conventionally Used for Hydrogen Embrittlement Study. *ECS Trans.* **2017**, *75*, 23–31. [CrossRef]
40. Akiyama, E.; Li, S. Electrochemical hydrogen permeation tests under galvanostatic hydrogen charging conditions conventionally used for hydrogen embrittlement study. *Corros. Rev.* **2016**, *34*, 103–112. [CrossRef]
41. Henriksen, J.F. The distribution of NaCl on Fe during atmospheric corrosion. *Corros. Sci.* **1969**, *9*, 573–576. [CrossRef]
42. Cho, S.W.; Ko, S.J.; Yoo, J.S.; Yoo, Y.H.; Song, Y.K.; Kim, J.G. Effect of Cr on aqueous and atmospheric corrosion of automotive carbon steel. *Materials* **2021**, *14*, 2444. [CrossRef]